REPORT DOCUMENTATION PAGE

Form Approved
OMB No. 0704-01-0188

PLEASE DO NOT RETURN YOUR FORM TO THE ABOVE ADDRESS.

1. REPORT DATE *(DD-MM-YYYY)*	2. REPORT TYPE	3. DATES COVERED *(From - To)*
11-06-2009	REPRINT	

4. TITLE AND SUBTITLE

Storm time global thermosphere: A driven-dissipative thermodynamic system

5a. CONTRACT NUMBER

5b. GRANT NUMBER

5c. PROGRAM ELEMENT NUMBER
62601F

6. AUTHORS
W. J. Burke*, C. S. Lin, M. P. Hagan*, Cheryl Y. Huang
D. R. Weimer**, J. O. Wise, L. C. Gentile*, and F. A. Marcos

5d. PROJECT NUMBER
2301

5e. TASK NUMBER
SD

5f. WORK UNIT NUMBER
A5

7. PERFORMING ORGANIZATION NAME(S) AND ADDRESS(ES)

Air Force Research Laboratory /RVBXP
29 Randolph Road
Hanscom AFB, MA 01731-3010

8. PERFORMING ORGANIZATION REPORT NUMBER
AFRL-RV-HA-TR-2010-1080

9. SPONSORING/MONITORING AGENCY NAME(S) AND ADDRESS(ES)

10. SPONSOR/MONITOR'S ACRONYM(S)
AFRL/RVBXP

11. SPONSOR/MONITOR'S REPORT NUMBER(S)

12. DISTRIBUTION/AVAILABILITY STATEMENT
Approved for public release; distribution unlimited.

13. SUPPLEMENTARY NOTES Reprinted From: Journal of Geophysical Research, Vol. 114, A06306, doi:10.1029/2008JA013848, 2009

 *Boston College Institute for Scientific Research, Chestnut Hill, MA 02467
**Solana Scientific, Inc., New Hampshire, now at Virginia Tech National Institute of Aerospace, Hampton, VA 23666

14. ABSTRACT

Orbit-averaged mass densities $\bar{\rho}$ and exospheric temperatures $\bar{T}_\infty$ inferred from measurements by accelerometers on the Gravity Recovery and Climate Experiment (GRACE) satellites are used to investigate global energy E_{th} and power Π_{th} inputs t the thermosphere during two complex magnetic storms. Measurements show $\bar{\rho}$, $\bar{T}_\infty$, and E_{th} rising from and returning to prevailing baselines as the magnetospheric electric field ε_{VS} and the Dst index wax and wane. Observed responses of E_{th} and $\bar{T}_\infty$ to ε_{VS} driving suggest that the storm time thermosphere evolves and a driven-but-dissipative thermodynamic system, described by a first-order differential equation that is identical in form to that governing the behavior of Dst. Coupling and relaxation coefficients of the E_{th}, $\bar{T}_\infty$, and Dst equations are established empirically. Numerical solutions of the equations for $\bar{T}_\infty$ and E_{th} are shown to agree with GRACE data during large magnetic storms. Since $\bar{T}_\infty$ and Dst have the same ε_{VS} driver, it is possible to combine their governing equations to obtain estimates of storm time thermospheric parameters even when lacking information about interplanetary conditions. This approach has the potential for significantly improving the performance of operational models used to calculate trajectories of satellites and space debris and is also useful for developing forensic reconstructions of past magnetic storms. The essential correctness of the approach is supported by agreement between thermospheric power inputs calculated from both GRACE-based estimates of E_{th} and the Weimer Poynting flux model originally derived from electric and magnetic field measurements acquired by the Dynamics Explorer 2 satellite.

15. SUBJECT TERMS
Magnetic storm Poynting flux Thermospheric energy

16. SECURITY CLASSIFICATION OF:			17. LIMITATION OF ABSTRACT	18. NUMBER OF PAGES	19a. NAME OF RESPONSIBLE PERSON
a. REPORT	b. ABSTRACT	c. THIS PAGE			Cheryl Huang
UNCL	UNCL	UNCL	UNL	9	19B. TELEPHONE NUMBER *(Include area code)*

JOURNAL OF GEOPHYSICAL RESEARCH, VOL. 114, A06306, doi:10.1029/2008JA013848, 2009

Storm time global thermosphere: A driven-dissipative thermodynamic system

W. J. Burke,[1,2] C. S. Lin,[1] M. P. Hagan,[2] C. Y. Huang,[1] D. R. Weimer,[3,4] J. O. Wise,[1] L. C. Gentile,[2] and F. A. Marcos[1]

Received 22 October 2008; revised 7 January 2009; accepted 1 April 2009; published 11 June 2009.

[1] Orbit-averaged mass densities $\overline{\rho}$ and exospheric temperatures $\overline{T}_\infty$ inferred from measurements by accelerometers on the Gravity Recovery and Climate Experiment (GRACE) satellites are used to investigate global energy E_{th} and power Π_{th} inputs to the thermosphere during two complex magnetic storms. Measurements show $\overline{\rho}$, $\overline{T}_\infty$, and E_{th} rising from and returning to prevailing baselines as the magnetospheric electric field ε_{VS} and the Dst index wax and wane. Observed responses of E_{th} and $\overline{T}_\infty$ to ε_{VS} driving suggest that the storm time thermosphere evolves as a driven-but-dissipative thermodynamic system, described by a first-order differential equation that is identical in form to that governing the behavior of Dst. Coupling and relaxation coefficients of the E_{th}, $\overline{T}_\infty$, and Dst equations are established empirically. Numerical solutions of the equations for $\overline{T}_\infty$ and E_{th} are shown to agree with GRACE data during large magnetic storms. Since $\overline{T}_\infty$ and Dst have the same ε_{VS} driver, it is possible to combine their governing equations to obtain estimates of storm time thermospheric parameters, even when lacking information about interplanetary conditions. This approach has the potential for significantly improving the performance of operational models used to calculate trajectories of satellites and space debris and is also useful for developing forensic reconstructions of past magnetic storms. The essential correctness of the approach is supported by agreement between thermospheric power inputs calculated from both GRACE-based estimates of E_{th} and the Weimer Poynting flux model originally derived from electric and magnetic field measurements acquired by the Dynamics Explorer 2 satellite.

Citation: Burke, W. J., C. S. Lin, M. P. Hagan, C. Y. Huang, D. R. Weimer, J. O. Wise, L. C. Gentile, and F. A. Marcos (2009), Storm time global thermosphere: A driven-dissipative thermodynamic system, *J. Geophys. Res.*, *114*, A06306, doi:10.1029/2008JA013848.

1. Introduction

[2] The US Space Surveillance Network (SSN) is responsible for tracking and predicting the trajectories of thousands of space objects. Precise orbit determinations require accurate knowledge of existing distributions of mass in the thermosphere. The performance of operational models of the thermosphere needed to calculate drag forces is satisfactory during quiet times but degrades as geomagnetic activity increases. During the magnetic storm of March 1989 more than 1500 objects in the SSN catalog were temporarily lost. The destruction of *Feng Yun 1C* by an antisatellite weapon in January 2007 created more than 2500 new debris fragments in low Earth orbit (LEO). The potential for debris from *Feng Yun* and preexisting objects to inflict severe to catastrophic damage on spacecraft operating in LEO has refocused attention on the need to strengthen collision-avoidance capabilities [*Wright*, 2007]. This in turn requires improved specifications of thermospheric conditions during severe space weather events.

[3] This paper describes a new approach to specifying thermospheric dynamics that was developed at the Air Force Research Laboratory (AFRL) to support operational storm time drag calculations [*Bowman et al.*, 2008]. It extends three AFRL studies of ionosphere-thermosphere (IT) responses to external driving during magnetic storms. The first study, by *Huang and Burke* [2004], showed that during the main phases of large magnetic storms Defense Meteorological Satellite Program (DMSP) spacecraft encounter repeated episodes of intense (>1000 nT) magnetic perturbations at magnetic latitudes <60°. These events produce only weak (<100 nT) disturbances on the ground. Conservative estimates of the total electromagnetic energy deposited in the ionosphere over a typical 20-minute epi-

[1]Air Force Research Laboratory, Space Vehicles Directorate, Hanscom AFB, Massachusetts, USA.
[2]Institute for Scientific Research, Boston College, Chestnut Hill, Massachusetts, USA.
[3]Solana Scientific, Inc., New Hampshire, USA.
[4]Now at Virginia Tech National Institute of Aerospace, Hampton, Virginia, USA.

0148-0227/09/2008JA013848$09.00

sode were a few percent of the ring current energy determined from the Dessler-Parker-Sckopke relation [*Carovillano and Siscoe*, 1973; *Stern*, 2005]. *Huang and Burke* [2004] concluded that: (1) models that rely on data from ground magnetometers at auroral latitudes greatly underestimate IT energy inputs, and (2) the ring current acts as an energy reservoir for heating the storm time thermosphere.

[4] The second AFRL study compared these conclusions with the dynamics of neutral densities inferred from measurements of accelerometers on the Gravity Recovery and Climate Experiment (GRACE) satellites during the storms of November 2004 [*Burke et al.*, 2007a]. This purely observational study yielded five empirical conclusions:

[5] 1. Consistent with conclusion (1) of *Huang and Burke* [2004], present drag models use the ap index as a driver and underestimate observed storm time density increases by >100%.

[6] 2. While crossing the polar cap near the noon-midnight meridian GRACE experienced unpredicted large positive and negative drag spikes as the spacecraft encountered head and tail winds driven by antisunward convecting ions.

[7] 3. Local densities ρ vary widely but orbital averages $\overline{\rho}$ evolve systematically during storms.

[8] 4. Magnetospheric electric fields $\varepsilon_{VS} \approx \Phi_{PC}/2L_YR_E$ predicted from parameters observed at L_1 anticipate variations of $\overline{\rho}$ with ~5 hr lead times. The symbols Φ_{PC} and $2L_YR_E$ represent the polar cap potential and width of the magnetosphere, respectively. L_Y is the distance in R_E from the Earth's center to the magnetopause along the dawn or dusk meridian.

[9] 5. During main and early recovery phases of storms the Dst index tracked $\overline{\rho}$ variations. From storm to storm, when $\varepsilon_{VS} \rightarrow 0$, $\overline{\rho}$ relaxed to prestorm levels at about the same rate. Dst returned to quiet time values at a much slower pace.

[10] Since the Dst and ap indices mostly reflect ground effects of magnetospheric and ionospheric Hall currents, respectively, and magnetospheric electric fields energize ring current particles, conclusions (1), (4), and (5) seemed to confirm the essential correctness of the ring current reservoir hypothesis. Allowing for local "density spikes" represented by (2), the systematic variations of $\overline{\rho}$ confirmed a suggestion of *Wilson et al.* [2006] that, on a global scale, the storm time thermosphere evolves as a large thermodynamic system that never strays far from diffusive equilibrium.

[11] *Wilson et al.* [2006] analyzed neutral densities inferred via the High Accuracy Satellite Drag Model (HASDM) [*Casali and Barker*, 2002] during all geomagnetic disturbances in the first six months of 2001. HASDM assimilates drag measurements from 75 calibration satellites with perigees ranging in altitude from 200 to 800 km. Consistent with the first law of thermodynamics, storm time variations in $\overline{\rho}$ reflect the thermal and gravitational energy histories of the thermosphere. Compiled energy histories derived from HASDM outputs were shown to be in substantial agreement with power into the high-latitude ionosphere predicted by the Poynting flux model of *Weimer* [2005] (W5). The W5 model combines statistically determined, high-latitude electrostatic and magnetic Euler potential responses to interplanetary changes to estimate Poynting fluxes into the global ionosphere and thermosphere. As such it does not require prior knowledge about distributions of ionospheric conductance. Because some fraction of the energy deposition occurs at altitudes below 200 km, W5 predictions exceeded HASDM-based calculations.

[12] In the third AFRL study *Burke* [2008] explored relationships implicit within the model of *Jacchia* [1977] (J77) to quantify thermospheric energy budgets during large magnetic storms. The choice of J77 was one of convenience; in principle these techniques can be adapted to any model. The J77 model uses analytic diffusion formulas to calculate density (ρ) and temperature (T) profiles for any exospheric temperature (T_∞). Appendix A provides the J77 equations used to specify temperature profiles. Exospheric temperatures T_∞ uniquely specify both density and temperature profiles. The modeled atmosphere consists of a fixed number of diatomic (N_2, O_2) and monatomic (O, Ar, He, H) species (σ). At altitudes $\leq$90 km, species are well mixed and maintain approximately the ground fractional densities. A minimum temperature of 188 K is assigned at the mesopause altitude h = 90 km. Above 90 km all species are in diffusive equilibrium specified by T(h) profiles that pass through inflection points at 125 km and approach T_∞ at high altitudes. For energy calculations below we define: number densities $n(r) = \sum_\sigma n_\sigma(r)$, mean masses $\overline{m}(r) = \frac{1}{n(r)} \sum_\sigma m_\sigma n_\sigma\ (r)$, mass densities $\overline{\rho}(r) = \overline{m}(r)n(r)$ and the heat capacity

$$C_V(r) \approx \frac{k_B A}{n(r)} \cdot \left\{ \frac{5}{2}(n[N_2] + n[O_2]) + \frac{3}{2}(n[O] + n[Ar] + n[He] + n[H]) \right\} \quad (1)$$

where $r = R_E + h$ is distance from the Earth's center; k_B and A are Boltzmann's constant and Avogadro's number, respectively. The approximation sign in equation (1) recognizes the absence of chemical reactions in the J77 thermosphere. In the model, height profiles of ρ and T are uniquely specified by T_∞. Since $\overline{\rho}$ is measured and the orbit-averaged altitude ($\overline{h}$) of GRACE is known, it seemed possible to use these two parameters to determine T_∞. Least squares testing revealed relationships between T_∞ and $\rho(h)$ found in J77 tables that are well represented in the form of a quadratic polynomial

$$T_\infty = \sum_{i=0}^{2} a_i(\overline{h})\rho^i(\overline{h}) \quad (2)$$

In the $300 \leq \overline{h} \leq 500$ km altitude range sampled by the GRACE and Challenging Minisatellite Payload satellites, the coefficients $a_i(h)$ are described by 5th-order polynomials.

$$a_i(\overline{h}) = \sum_{j=0}^{5} b_{ij}\overline{h}^j \quad (3)$$

Specifically

$$\begin{pmatrix} a_0(\bar{h}) \\ a_1(\bar{h}) \\ a_2(\bar{h}) \end{pmatrix} = \begin{pmatrix} -28.10 & 2.69 & -2.03 \times 10^{-3} & 0 & 0 & 0 \\ -4.733 \times 10^{17} & 4.312 \times 10^{15} & -1.372 \times 10^{13} & 1.60 \times 10^{10} & 0 & 0 \\ 3.2695 \times 10^{32} & -4.620 \times 10^{30} & 2.618 \times 10^{28} & -7.456 \times 10^{25} & 1.071 \times 10^{23} & -6.237 \times 10^{19} \end{pmatrix} \times \begin{pmatrix} 1 \\ \bar{h} \\ \bar{h}^2 \\ \bar{h}^3 \\ \bar{h}^4 \\ \bar{h}^5 \end{pmatrix} \quad (4)$$

Regression coefficients obtained in fitting T_∞ and a_i to polynomials exceed 0.999. In applying equations (2), (3) and (4), $\bar{\rho}$ and $\bar{h}$ are in grams/cc and kilometers, respectively.

[13] The total thermospheric energy density is the sum of the thermal $\eta_T(r) = C_V(r)n(r)T(r)/A$, and potential energy contributions $\phi_G(r) = \rho(r)M_E G/r$ [*Wilson et al.*, 2006]. The symbols M_E and G represent the Earth's mass and the gravitational constant, respectively. To estimate the thermosphere's total energy content $E_{th} = H_T + \Phi_G$, it is necessary to integrate $\eta_T(r)$ and $\phi_G(r)$ over the volume of the thermosphere. Our use of $\bar{\rho}$ has effectively averaged latitudinal variations of the integrands. Local time integrations are effected via considerations of exospheric temperature distributions in the Jacchia models where T_∞ ranges between some minimum and maximum values with a ratio of $R \approx 1.31$. Polar-orbiting spacecraft like GRACE sample globally averaged exospheric temperatures $\bar{T}_\infty \approx 1.155 T_{\infty\,\min}$ regardless of the local times of their orbital planes. Note that current drag models determine the parameter $T_{\infty\,\min}$ from combinations of average and present levels of solar EUV radiance proxies and the prevailing ap index [*Bowman et al.*, 2006]. The total *thermal* energy is approximately

$$H_T \approx 4\pi \int_{R_E+h_0}^{R_E+1000} \eta(r) r^2 dr = \frac{4\pi}{A} \int_{R_E+h_0}^{R_E+1000} C_V(r) n(r) T(r) r^2 dr \quad (5)$$

Since we are only interested in changes in potential energy it is useful to set the potential energy of the thermosphere to zero at the base of the integration range [*Wilson et al.*, 2006] and represent the *gravitational* energy of thermospheric neutrals as

$$\Phi_G \approx 4\pi \int_{R_E+h_0}^{R_E+1000} [\phi(r) - \phi(r_0)] r^2 dr$$
$$= 4\pi M_E G \int_{R_E+h_0}^{R_E+1000} \rho(r) \left[\frac{1}{r} - \frac{1}{r_0}\right] r^2 dr \quad (6)$$

With information available in J77 tables, *Burke* [2008] calculated the integrands of (5) and (6) for $700 \le T_\infty \le 2000$ K at increments of 100 K then numerically integrated them upward from an altitude of 100 km to obtain E_{th} as a function of T_∞. A linear regression analysis of the resulting E_{th} as a function of $\bar{T}_\infty$ showed that

$$E_{th}(h \ge 100\,\text{km}) = 5.365\,10^{17} + 8.727\,10^{13}\bar{T}_\infty \quad (7)$$

with a regression coefficient $R > 0.998$. We see that if $\bar{T}_\infty$ changes by 100 K, E_{th} gains/loses $\sim 8.7 \cdot 10^{15}$ J. Over the range $700 \le T_\infty \le 2000$ K, E_{th} only varies by $\sim 15\%$.

[14] The following section briefly describes data sources used in this report. The third section presents orbital averaged densities measured by GRACE during the summer and late autumn of 2004, as well as exospheric temperatures and thermospheric energies derived from them via J77. These parameters are compared with Dst and ε_{VS}. Our analysis of GRACE data indicates that storm time E_{th} relaxes exponentially to predisturbance levels when ε_{VS} turns off. In the fourth section we treat E_{th}, T_∞, and Dst as manifestations of driven-dissipative systems with the same ε_{VS} driver and compare predictions with available observations. The fifth section contains a summary of research presented in this paper, a list of its new conclusions, and offers comments on the limits of applicability for coupling coefficients derived from GRACE measurements. The document also contains two appendices that describe the J77 model and the derivation of ε_{VS}.

2. Data Sources

[15] Thermospheric mass densities are estimated from measurements of nearly identical Spatial Triaxial Accelerometer for Research (STAR) sensors on CHAMP and two GRACE satellites that fly in tandem in nearly circular, polar orbits [*Tapley et al.*, 2004]. STAR sensors monitor electrostatic forces needed to maintain proof masses (PM) at the center of cages located within 2 mm of each spacecraft's center of mass [*Bruinsma et al.*, 2004]. The spacecraft and PM respond to gravity in the same way. Thus changes in the electrostatic forces that maintain the PM at the center of its cage reflect spacecraft responses to nongravitational forces such as atmospheric drag and radiation pressure [*Bruinsma and Biancale*, 2003]. Acceleration due to atmospheric drag is given by

$$a_{drag} = C_D(A_{sc}/M_{sc})\rho V^2 \quad (8)$$

where A_{sc} and M_{sc} represent the cross-sectional area and mass of the spacecraft, respectively, ρ the mass density of the neutral atmosphere, and V is the spacecraft velocity in the rest frame of ambient neutrals. The drag coefficient C_D depends on the angle of flow to the spacecraft surface, the ratio of the temperatures of the satellite surface and the local atmosphere, and the ratio of the mean mass of atoms in the atmosphere to those on the satellite surface [*Bruinsma and Biancale*, 2003].

[16] To maintain the same temporal cadence as Dst, ε_{VS} values presented in this paper were calculated using hourly averaged values of solar wind and IMF parameters from the

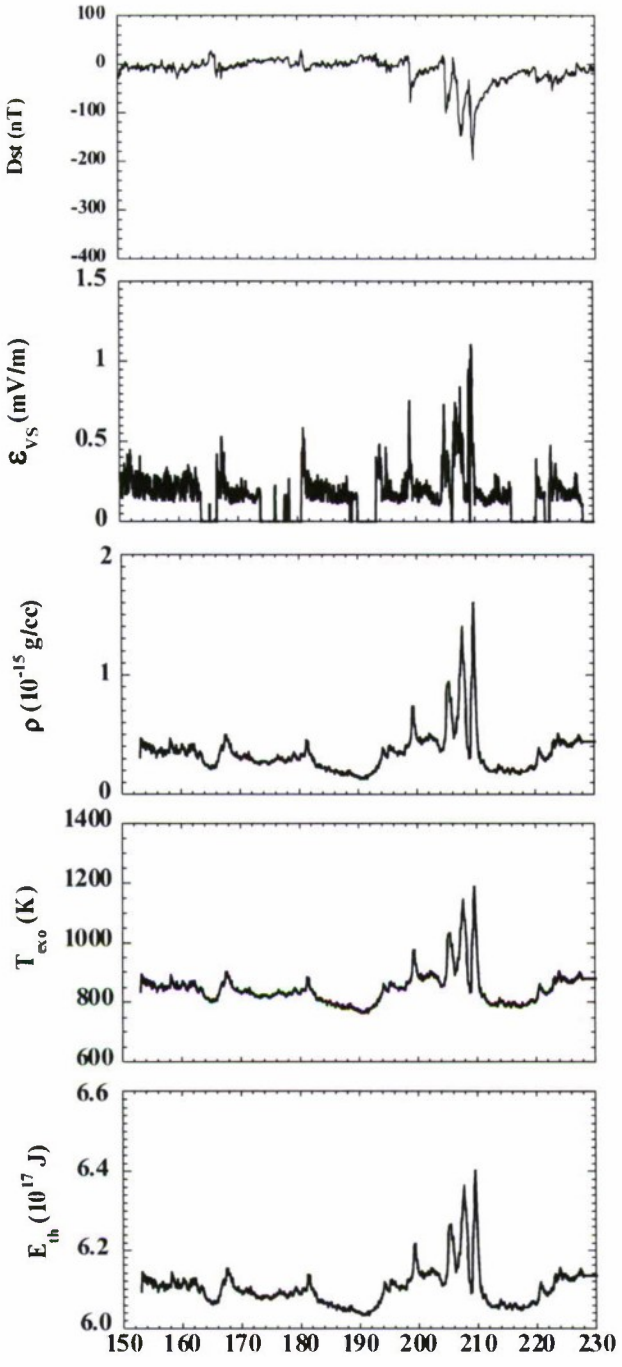

Figure 1. Geophysical parameters and thermospheric responses observed by GRACE. From top to bottom, plots show the history of the Dst index, ε_{VS}, as well as orbit-averaged measurements of mass density $\overline{\rho}$, exospheric temperature $\overline{T}_\infty$ and thermospheric energy E_{th}. Data are plotted as functions of universal time from Julian days 150 to 230, 2004.

Advanced Composition Explorer (ACE) satellite in a halo orbit around the L_1 point, ~234 R_E upstream of Earth. The solar wind density and velocity are measured by the Solar Wind Electron, Proton, and Alpha Monitor (SWEPAM) [*McComas et al.*, 1998]. The interplanetary magnetic field (IMF) vector is observed by the magnetic field instrument (MFI) [*Smith et al.*, 1998].

3. GRACE Observations

[17] Figure 1 includes plots of the geophysical parameters Dst (top) and ε_{VS} (second) as well as orbit-averaged measurements of $\overline{\rho}$ (third), $\overline{T}_\infty$ (fourth), and E_{th} (bottom) acquired by GRACE between 1 June and 17 August 2004 (Julian days (JD) 150 to 230). During this interval GRACE's orbit-averaged altitude was ~486.5 km; its orbital plane precessed from near the noon-midnight to the dawn-dusk meridian. Values of $\overline{T}_\infty$ and E_{th} were obtained by applying equations (2) and (7) to the $\overline{\rho}(t)$ stream. The data plots show that $\overline{T}_\infty$ ranged from 750 to 1200 K and E_{th} between 6.05 and $6.4 \cdot 10^{17}$ J over this period.

[18] Last three data plots in Figure 1 show that $\overline{\rho}(t)$, $\overline{T}_\infty$ and E_{th} vary on two time scales: (1) low-frequency variations with the 27-day solar rotation, and (2) outerops that emerge in response to changes in geophysical conditions related to intensifications of Dst and ε_{VS}. The largest change in the E_{th} trace of $\sim 3 \cdot 10^{16}$ J occurred on JD 209 in response to interplanetary forcing when Dst attained a minimum value of about −200 nT. The energy of the ring current E_{RC} estimated via the Dessler-Parker-Sckopke (DPS) relation [*Stern*, 2005] is

$$E_{RC}(J) \approx \frac{3E_M Dst}{2B_0} \approx 2.58 \cdot 10^{13}\ Dst(nT) \qquad (9)$$

where $B_0 \approx 3.1 \cdot 10^4$ nT is the magnetic field at the equator, and $E_M \approx 8 \cdot 10^{17}$ J is the energy of the magnetic field above the Earth's surface. Equation (9) indicates that at its maximum value $E_{RC} \approx 5.16 \cdot 10^{15}$ J and was substantially smaller than the increase in E_{th}. This empirical result indicates that the ring current reservoir hypothesis is untenable. A large fraction of the storm time energy budget comes from the solar wind to the thermosphere, unmediated by the ring current.

[19] Figure 2 compares the same geophysical and GRACE parameters measured during JD 305–330 (2–27 November 2004) using the format of Figure 1. The orbital plane of GRACE was near the noon-midnight meridian. The Dst plot shows that two major geomagnetic disturbances occurred between JD 312 and 315 (7–10 November). Similar disturbances appear on all of the other plots. Dst minima were −373 nT (06:00 UT, 8 November) and −289 nT (10:00 UT, 10 November). The corresponding values of E_{RC} are 9.62 and $7.46 \cdot 10^{15}$ J; predisturbance baselines for $\overline{T}_\infty$ and E_{th} were near 900 K and $6.15 \cdot 10^{17}$ J, respectively. $\overline{T}_\infty$ rose to 1390 K at 07:00 UT on JD 313 and 1350 K at 10:00 UT on JD 315. E_{th} maxima at these times were 6.58 and $6.52 \cdot 10^{17}$ J. Again, corresponding ΔE_{th} values of 4.3 and $3.7 \cdot 10^{16}$ J exceed estimates of E_{RC} 9.6 and $7.5 \cdot 10^{15}$ J, respectively.

[20] *Burke et al.* [2007a] found that storm time thermospheric density increases always relaxed at the same rate when ε_{VS} turned off. It turns out that the storm time thermosphere loses its storm time energy increment exponentially with time. This is demonstrated in Figure 3 in which ε_{VS} and the natural logarithm of E_{th} are plotted as functions of UT during the disturbed interval JD 204–211 (22–29 July 2004). Vertical lines mark times when ε_{VS}

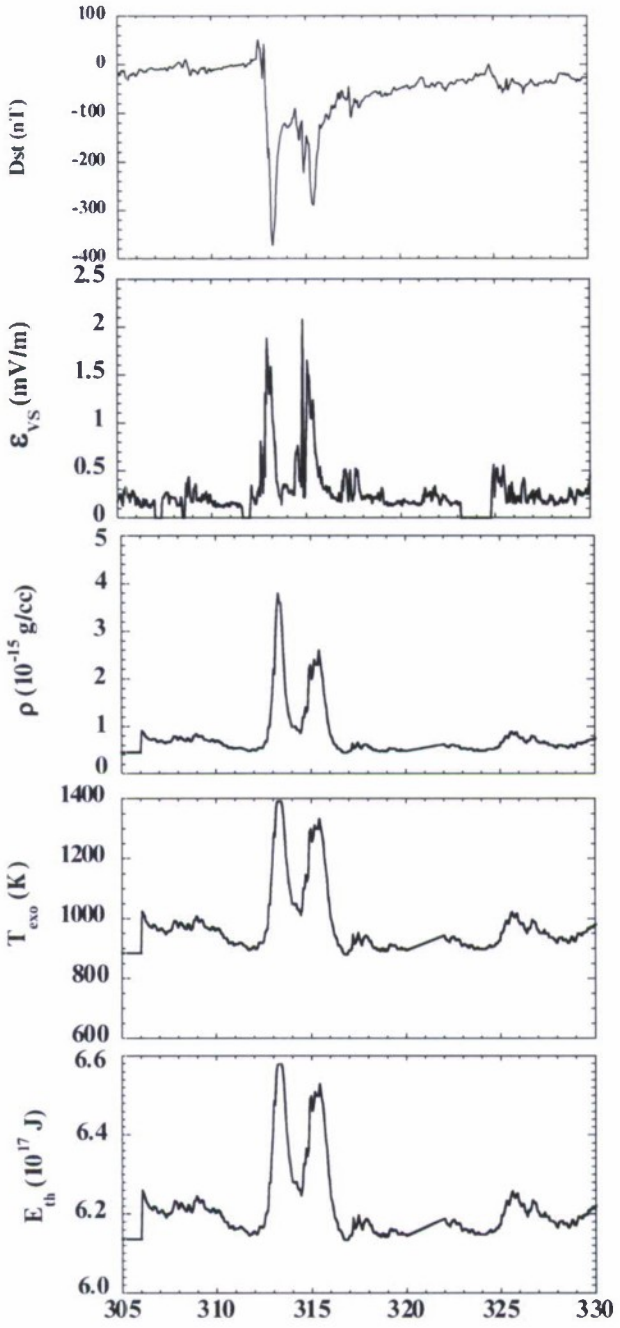

Figure 2. Geophysical parameters and thermospheric responses observed by GRACE plotted as functions of time for JD 306 to 330, 2004 using the same format as Figure 1.

rapidly decreased to low values. The two slanted lines that overlay the trace of ln E_{th} during the subsequent periods of low ε_{VS} have identical slopes. Numerically, E_{th} has an e-fold relaxation time $\tau \approx 6.5$ hours.

4. Modeling a Driven-Dissipative Thermosphere

[21] The behavior of E_{th}, responding to variations in ε_{VS} and decaying exponentially to predisturbance levels when it turns off, is reminiscent of commonly observed phenomena called driven-dissipative systems. The magnetic energy generated by a current flowing in a resistor-inductor (R-L) circuit provides a familiar example [*Young*, 1992]. *Burton et al.* [1975] proposed that the ring current evolves in a similar way and derived a linear differential that describes changes in Dst*, the pressure corrected Dst.

$$\frac{dDst^*}{dt} = \alpha_D \varepsilon_I - \frac{Dst^*}{\tau_{RC}} \tag{10}$$

Here ε_I, α_D, and τ_{RC} represent the interplanetary electric field, the coupling coefficient and the relaxation time constant of the ring current, respectively.

[22] The following subsections consider the driven-dissipative properties of E_{th}, T_∞, and Dst. The analogy of rolling hills and rocky outcrops drawn from GRACE data in Figure 1 indicates that we may regard the scalar fields E_{th} and T_∞ as having two independent additive sources, the solar EUV radiance and the solar wind. The driven-dissipative equations presented below describe the solar wind contributions to these scalars.

4.1. Energy and Power

[23] During magnetic disturbances E_{th} variations correlate with ε_{VS}. Rather than pursue statistical relationships between these two quantities, we propose to exploit implications of information contained in the decay characteristics of E_{th} illustrated in Figure 3. Specifically we postulate that on a global scale the storm time thermosphere acts like a driven-dissipative system. If this conjecture is correct, the solar wind contribution to E_{th} should evolve in ways similar to Dst in equation (10). The governing equation takes the form

$$\frac{dE_{th\,SW}}{dt} = \alpha_E \varepsilon_{VS} - \frac{E_{th\,SW}}{\tau_E} \tag{11}$$

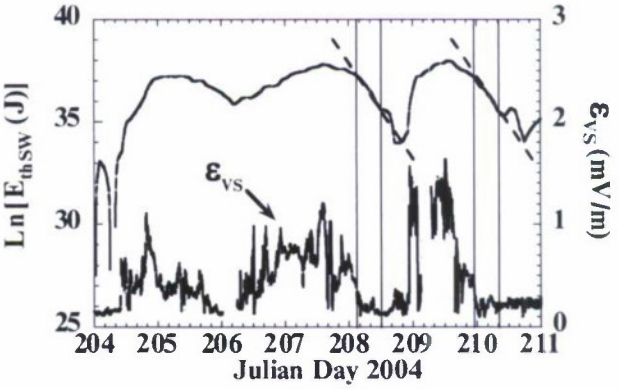

Figure 3. Plots of ε_{VS} and the natural logarithm of $E_{th\,SW}$ for the disturbance on JD 206 to 211, 2004. Vertical lines mark times of electric field decrease. The slanted lines have the same slopes indicating that $E_{th\,SW}$ decays exponentially when ε_{VS} turns off. The estimated e-fold relaxation time τ is ~6.5 hours.

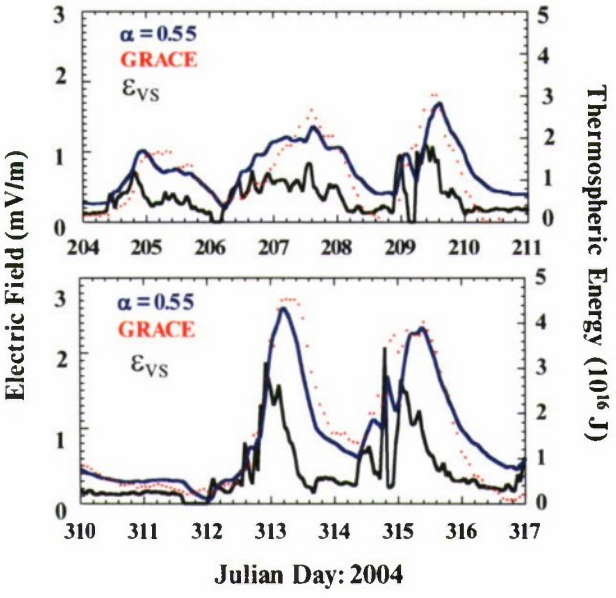

Figure 4. Comparison of ε_{VS} (black), modeled $E_{th\ SW}$ (blue), and $E_{th\ SW}$ values inferred from GRACE measurements of $\overline{\rho}$ (red dots) plotted as functions of universal time during magnetically disturbed periods of (top) July and (bottom) November 2004. $E_{th\ SW}$ is plotted in units of 10^{16} J.

The coupling constant α_E and relaxation time τ_E = 6.5 hours are empirically determined. Equation (7) can be solved numerically

$$E_{th\,SW}(t_{n+1}) = \alpha_E \varepsilon_{VS}(t_n)\Delta t + E_{th\,SW}(t_n)\left(1 - \frac{\Delta t}{\tau_E}\right) \qquad (12)$$

where Δt represents the time step between samples. For convenience we let Δt = 1 hour, and express ε_{VS} in mV/m. In this case

$$\begin{aligned} E_{th\,SW}(t_{n+1}) &= \alpha_E \varepsilon_{VS}(t_n) + E_{th\,SW}(t_n)\left(1 - \frac{1}{\tau_E}\right) \\ &= \alpha_E \varepsilon_{VS}(t_n) + .846 E_{th\,SW}(t_n) \end{aligned} \qquad (13)$$

Through trial and error comparisons with GRACE measurements acquired during JD 150–230, 2004 we found that $\alpha_E \approx 5.5 \cdot 10^{15}$ [(J/hr)/(mV/m)]. Numerical solutions of equation (13) can be compared with GRACE measurements to confirm or refute the assumption.

[24] Figure 4 contains plots of ε_{VS} (black), solutions of equation (13) (blue) and GRACE measurements of $E_{th\ SW}$ (red). The plots represent the disturbed periods in (top) July and (bottom) November 2004. In both instances we approximated $E_{th\ SW}$ as $E_{th} - 6.1 \cdot 10^{17}$ J since the $E_{th\ SW}$ calculations in Figure 5 are presented in units of 10^{16} J. Although α_E was determined using data from the summer of 2004 only, predictions of equation (13) also appear to be in good agreement with GRACE measurements during November 2004.

[25] The essential correctness of equation (13) can also be verified or falsified by comparing GRACE observations of thermospheric energy changes with independent W5 predictions of electromagnetic power into the thermosphere. W5 uses solar wind/IMF measurements to predict distributions of Poynting flux into the northern and southern ionospheres. Integration over the affected areas provides the global rates of energy input P_{W5}. On the other hand, orbit-averaged E_{th} measurements from GRACE are snapshots that capture the thermosphere's total energy content averaged over orbital periods. GRACE data reflect balances that the thermosphere strikes between power received from the solar wind and lost via radiative and other processes [*Mlynczak et al.*, 2005].

[26] Equation (11) provides a bridge between the two approaches. The term $\alpha_E \varepsilon_{VS}$ represents the rate at which energy is provided to drive the storm time thermosphere. Thus it can be compared with P_{W5} directly. Since $\alpha_E \approx 5.5 \cdot 10^{15}$ [(J/hr)/(mV/m)] and P_{W5} is in Watts we must divide α_E by 3600 s/hr to obtain $\alpha_E \approx 1.528 \cdot 10^{12}$ W/(mV/m) or 1.528 TW/(mV/m). Figure 5 shows plots of P_{W5} (red) at a 5-minute cadence and hourly averaged $\Pi_{th} \approx \alpha_E \varepsilon_{VS}$ in TW for the storms of July and November 2004. The $\alpha_E \varepsilon_{VS}$ trace was time shifted by 1 hour to allow for transport from ACE to the magnetosphere. Delay times used in W5 vary according to the speed of the solar wind and the tilt angle of surfaces of constant interplanetary electric field phase [*Weimer et al.*, 2002]. In general the agreement between P_{W5} and the power required to explain GRACE-based calculations of E_{th} appears remarkably good. Thus, on a

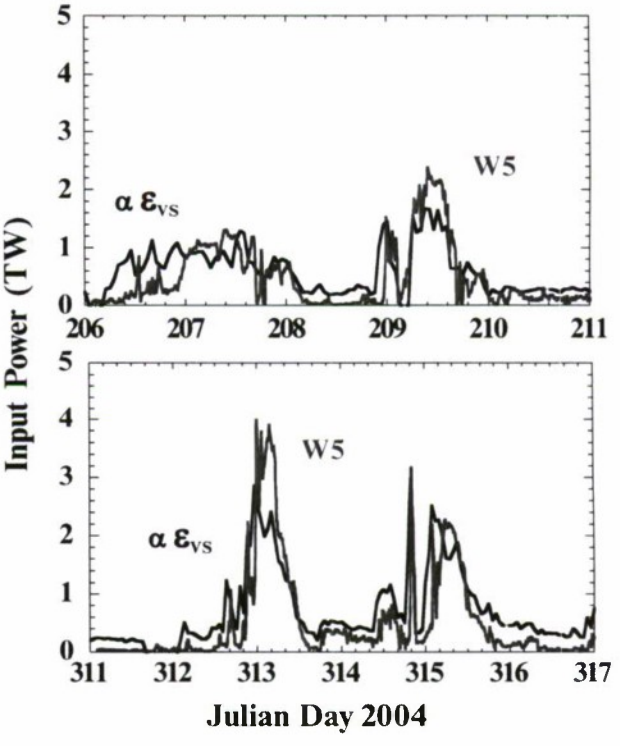

Figure 5. Comparison of storm time power into the global thermosphere predicted by the W5 model (red) and $\alpha\varepsilon_{VS}$ (black) plotted as functions of UT during magnetically disturbed periods in (top) July and (bottom) November 2004.

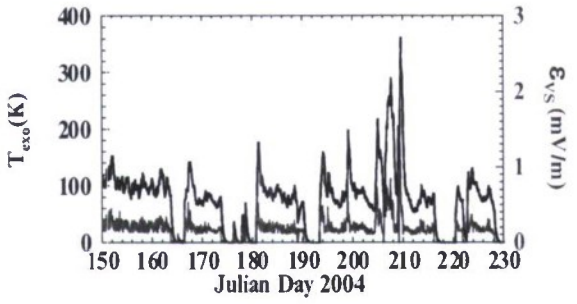

Figure 6. Model predictions of $T_{\infty\ SW}$ (black) and ε_{VS} (red) inferred from hourly averaged parameters from ACE, plotted as functions of universal time for JD 150 to 230, 2004.

global scale, power inputs predicted by W5 and needed to model GRACE measurements are viewed as mutually consistent. Consequently, P_{W5} as well as $\alpha_E\ \varepsilon_{VS}$ can be used as a driver in equation (11) to estimate the development of $E_{th\ SW}$.

[27] Attention is directed to two particular aspects of the results shown in Figure 5.

[28] 1. GRACE measurements and W5 predictions indicate sustained electromagnetic power input $\geq$1 TW during both the July and November storms. This is significantly greater than the storm time inputs due to energetic particle precipitation and from solar UV [*Knipp et al.*, 2005].

[29] 2. During the third disturbance of the July period and the first one of the November storms, $P_{W5} > \alpha_E\ \varepsilon_{VS}$ by significant amounts. This discrepancy probably reflects the different estimates of Φ_{PC}. In both instances the polar cap potential used in W5 was larger than that predicted by the Siscoe-Hill model (Appendix A). For a given system of field-aligned currents the one driven by the higher Φ_{PC} requires a higher power input to overcome collisional drag exerted by neutrals on $\mathbf{E} \times \mathbf{B}$ drifting ions.

4.2. Exospheric Temperatures

[30] While E_{th} may be of interest for estimating energy transfer from the solar wind and magnetosphere to the thermosphere via the high-latitude ionosphere, $\overline{T}_\infty$ is generally a more useful parameter for operational modelers of atmospheric drag [*Marcos et al.*, 1998]. The linear relationship between E_{th} and $\overline{T}_\infty$ captured in equation (7) indicates that a differential equation similar to (11) also describes the evolution of $\overline{T}_{\infty SW}$. We assume that $\overline{T}_\infty$ has independent UV and solar wind sources, $\overline{T}_\infty = \overline{T}_{\infty\ UV} + \overline{T}_{\infty\ SW}$. Since the solar UV provides thermospheric baselines

$$\overline{T}_{\infty UV} = \frac{E_{th\,UV}(J) - 5.365 \cdot 10^{17}}{8.727 \cdot 10^{13}} \tag{14}$$

and

$$\overline{T}_{\infty\ SW} = \frac{E_{th\,SW}(J)}{8.727 \cdot 10^{13}} \tag{15}$$

substitution of (15) into (13) gives

$$\overline{T}_{\infty\ SW}(t_{n+1}) = \alpha_T \varepsilon_{VS}(t_n) + \overline{T}_{\infty\ SW}(t_n)\left(1 - \frac{1}{\tau_E}\right)$$
$$\approx 63\,\varepsilon_{VS}(t_n) + .846\,\overline{T}_{\infty\ SW}(t_n) \tag{16}$$

The coupling coefficient $\alpha_T = \alpha_E/8.727 \cdot 10^{13} = 5.5 \cdot 10^{15}/8.727 \cdot 10^{13} \approx 63$.

[31] Figure 6 shows plots of ε_{VS} (red) and $\overline{T}_{\infty\ SW}$ (black) for JD 150–230, 2004. Attention is directed to three aspects of these data:

[32] 1. Whenever solar wind data from ACE were unavailable we set $\varepsilon_{VS} = 0$. In these intervals modeled $\overline{T}_{\infty\ SW}$ decreased exponentially, but quickly recovered when the ε_{VS} data stream resumed.

[33] 2. During periods of relative magnetic quiet $\overline{T}_{\infty\ SW}$ ranged between 70 K and 100 K.

[34] 3. Spikes in ε_{VS} always produced analogous responses in $\overline{T}_{\infty\ SW}$.

[35] Figure 7 compares variations of modeled $\overline{T}_{\infty\ SW}$ (blue) with values inferred via equation (2) from measurements of $\overline{\rho}$ by accelerometers on GRACE during the two magnetic storm periods. For the July and November storms we estimated $\overline{T}_{\infty\ SW}$ by subtracting constant baseline estimates of 900 K from the full measured values of $\overline{T}_\infty$ shown in Figures 1 and 2. Again, agreement between model predictions and observations appears quite good. Closer agreement between data and the model can be achieved using time-varying representations of $\overline{T}_{\infty\ UV}$ baselines that allow for solar rotation induced trends apparent in GRACE data [*Bowman et al.*, 2008].

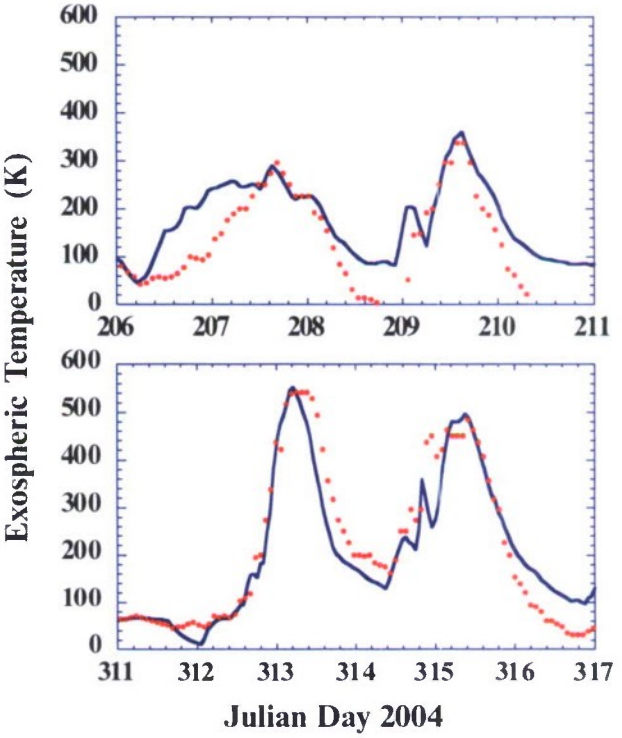

Figure 7. Modeled $\overline{T}_{\infty SW}$ (blue) and values inferred from GRACE measurements of $\overline{\rho}$ (red dots), plotted as functions of UT during the magnetically disturbed periods of (top) July and (bottom) November 2004. $\overline{T}_{\infty SW}$ was approximated by subtracting 850 K from GRACE-based estimates of T_∞.

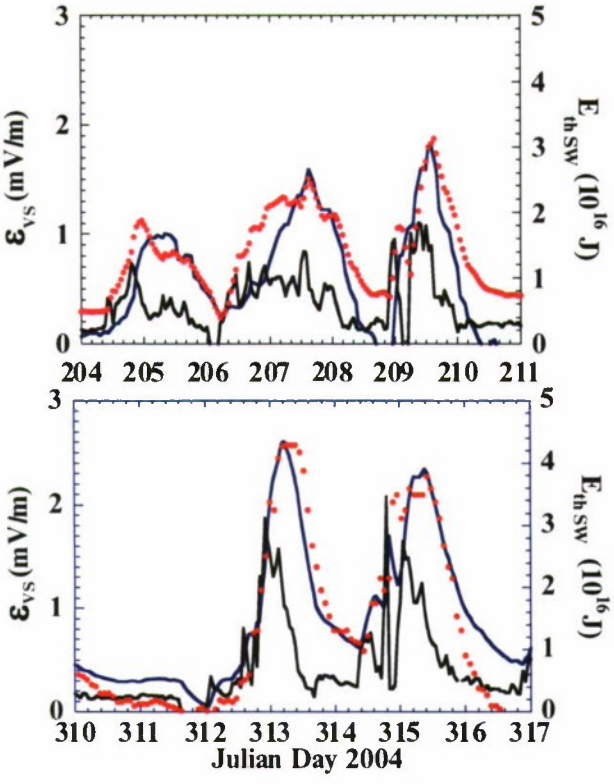

Figure 8. Comparison of (black), modeled (blue), and measured (red) Dst plotted as functions of UT during the magnetically disturbed periods of (top) July and (bottom) November 2004. For ease in making comparisons with ε_{VS}, plots show the negative of Dst.

4.3. Thermosphere-Dst Relationships

[36] *Burke et al.* [2007a] demonstrated that during magnetic storms the Dst index evolves in ways that closely approximate the forms of $\overline{\rho}(t)$ traces throughout the main and early recovery phases of storms. In late recovery phases Dst relaxes over several days while $\overline{\rho}(t)$ returns to its prestorm baseline in a few hours. *Burke et al.* [2007b] found that during magnetic storms with simple main phases, $Dst(t) = a + b \cdot I_{VS}(t)_t$ with very high correlation coefficients, where $I_{VS}(t) = \int_{t_0} \varepsilon_{VS}(t')dt'$. This approach ignores the main phase dissipation term in equation (10). Linear regression slopes varied over a relatively wide range. The steepest slopes of about −40 nT/(mV/m) were obtained during storms with sharp transitions between main and recovery phases. We approximate (10) as

$$\frac{dDst}{dt} = \alpha_D \varepsilon_{VS} - \frac{Dst}{\tau_{RC}} \tag{17}$$

using $\alpha_D = -40$ [(nT/hr)/(mV/m)] and $\tau_{RC} = 7.7$ hour [http://sprg.ssl.berkeley.edu/dst_ index/welcome.html]. This approach has two obvious advantages: (1) E_{th}, T_∞, and Dst can all be regarded as responding to the same force field, and (2) ε_{VS} approximates the electric field that energizes ring current particles and incorporates the essentially nonlinear coupling of the solar wind/IMF with the storm time magnetosphere (cf. Appendix B). To test the utility of making this substitution Figure 8 compares ε_{VS} (black) with solutions for equation (17) (blue) and provisional Dst (red) as functions of time during the July and November 2004 storms. While lacking the precision and sophistication of artificial intelligence solutions presented by *Temerin and Li* [2002, 2006] equation (17) gives an approximate representation of Dst's storm time development.

[37] Over the past decade the solar wind/IMF data needed to calculate ε_{VS} have been available almost continuously. However, critical input data were often unavailable in the past and may become so in the not-too-distant future. During many storms energetic solar protons render it impossible to determine solar wind densities in real time. Nevertheless operational responsibility for calculating the precise trajectories of space objects continues. Knowledge of T_∞ is critical for estimating thermospheric densities and the corresponding atmospheric drag (equation (8)). The remainder of this subsection explores the possibility of using Dst to provide real-time information regarding changes in T_∞ during magnetic disturbances.

[38] It is possible to exploit the formal similarities between differential equations for T_∞ and Dst to calculate the enhanced storm time drag on space objects even in the absence of data from L_1. This is accomplished by eliminating the common term ε_{VS} from the two equations

$$\frac{1}{\alpha_T}\left[\overline{T}_{\infty SW}(t_{n+1}) - \left(1 - \frac{1}{\tau_E}\right)\overline{T}_{\infty SW}(t_n)\right] = \varepsilon_{VS}(t_n) = \frac{1}{\alpha_D}\left[Dst(t_{n+1}) - \left(1 - \frac{1}{\tau_{RC}}\right)Dst(t_n)\right] \tag{18}$$

Rearranging terms gives

$$\overline{T}_{\infty SW}(t_{n+1}) = \left(1 - \frac{1}{\tau_E}\right)\overline{T}_{\infty SW}(t_n) + \frac{\alpha_T}{\alpha_D}\left[Dst(t_{n+1}) - \left(1 - \frac{1}{\tau_{RC}}\right)Dst(t_n)\right] \tag{19}$$

To solve (19) numerically we set $\overline{T}_{\infty\,SW}(t_0) = 0$; the ratio $\alpha_T/\alpha_D \approx 1.575$. Since we are only interested in the storm time Dst, following *Burton et al.* [1975] we set the "quiet time" Dst as −20 nT and impose the numerical constraint

$$Dst = \begin{array}{ll} Dst: & \text{if } Dst < -20nT \\ -20nT: & \text{if } Dst \geq -20nT \end{array} \tag{20}$$

Figure 9 plots calculated values of $\overline{T}_{\infty\,SW}(t)$ (blue) obtained using the Dst time series as the driver of equation (19). The red dots again represent values of $\overline{T}_{\infty\,SW} = \overline{T}_\infty - 900$ K inferred from GRACE measurements of $\overline{\rho}$. By and large agreement between the model and data appears quite good. Note that on JD 210 and 316 the modeled $\overline{T}_{\infty\,SW}(t)$ decays at a much slower rate than is actually observed. This reflects the slow decay rate of the symmetric ring current in the late main phase when electric coupling between the magnetosphere and ionosphere-thermosphere weakens. *Bowman et al.* [2008] describe practical ways to overcome this deficiency.

[39] It is also possible to apply this technique to make forensic reconstructions of thermospheric and interplanetary

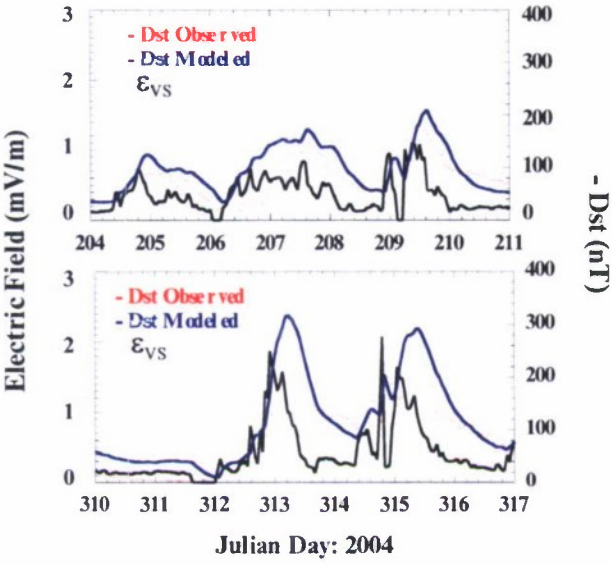

Figure 9. Predicted $T_{\infty\ SW}$ (blue) with Dst as driver and values inferred from density measurements by GRACE (red) plotted as functions of UT during the magnetically disturbed periods of (top) July and (bottom) November 2004. As in Figure 7, measured $T_{\infty\ SW}$ was approximated by subtracting 850 K from GRACE-based estimates of T_{∞}.

conditions during previous large magnetic disturbances when solar wind measurements were unavailable. Because of its widespread space weather effects the March 1989 storm offers an interesting example. The trace in the bottom plot of Figure 10 shows that early on 14 March Dst approached a minimum of −600 nT. Figure 10 (middle) shows $\overline{T}_{\infty\ SW}(t)$ obtained by a numerical solution of equation (19). We estimate that $\overline{T}_{\infty}$ rose ~800 K above prestorm background levels, much more than the 300 to 400 K increases of July and November 2004. Figure 10 (top) plots an estimate of ε_{VS} obtained through a numerical solution of equation (18). Near the maximum epoch of the main phase the calculated ε_{VS} exceeded 4 mV/m. Although this value is large in comparison with the July and November 2004 storms, it is not outlandish. During the storm of March 1991 the Combined Release and Radiation Effects Satellite (CRRES) measured sustained dawn-to-dusk electric fields of ~6 mV/m in the inner magnetosphere [*Wygant et al.*, 1998].

5. Discussion and Conclusions

[40] This section summarizes the research reported above, lists its three new scientific conclusions, and comments on its range of applicability.

[41] During the main phases of large magnetic storms DMSP spacecraft regularly cross sheets of intense (>1 A/m) field-aligned currents at auroral latitudes that produce very weak ground signatures. Energy deposited over the ~20-minute lifetimes of these structures accumulates to a significant fraction of the ring current energy. *Huang and Burke* [2004] suggested that: (1) models using ground magnetometer measurements underestimate energy inputs to the storm time thermosphere, and (2) the ring current acts as an energy reservoir from which the thermosphere draws energy. Direct comparisons of GRACE measurements with predictions of presently used models confirmed the first conclusion [*Burke et al.*, 2007a]. Observed correlations between variations of $\overline{\rho}$ and Dst/ε_{VS} seemed to confirm the second. In this paper we applied a new technique to determine exospheric temperatures and thermospheric energy contents from GRACE measurements of $\overline{\rho}$. Data presented in Figures 1 and 2 show that during large magnetic storms the energy content of the global thermosphere rises by several times that of the ring current estimated via the Dessler-Parker-Sckopke relation. The observed responses of E_{th} to ε_{VS} led us to explore the possibility that the storm time thermosphere and ring current act as driven-dissipative systems with the same driver but different relaxation time constants. Numerical solutions of the differential equation governing the behavior of such systems were compared with the observed variability of E_{th}, T_{∞}, and Dst. Agreement between data and model predictions confirms the essential correctness of the driven-dissipative perception. Given their widely different data sources, we regard agreement between estimates of electromagnetic power into the thermosphere predicted by $\alpha_E\varepsilon_{VS}$ and P_{WS} as strong, independent confirmation of our driven-dissipative perception of the storm time thermosphere.

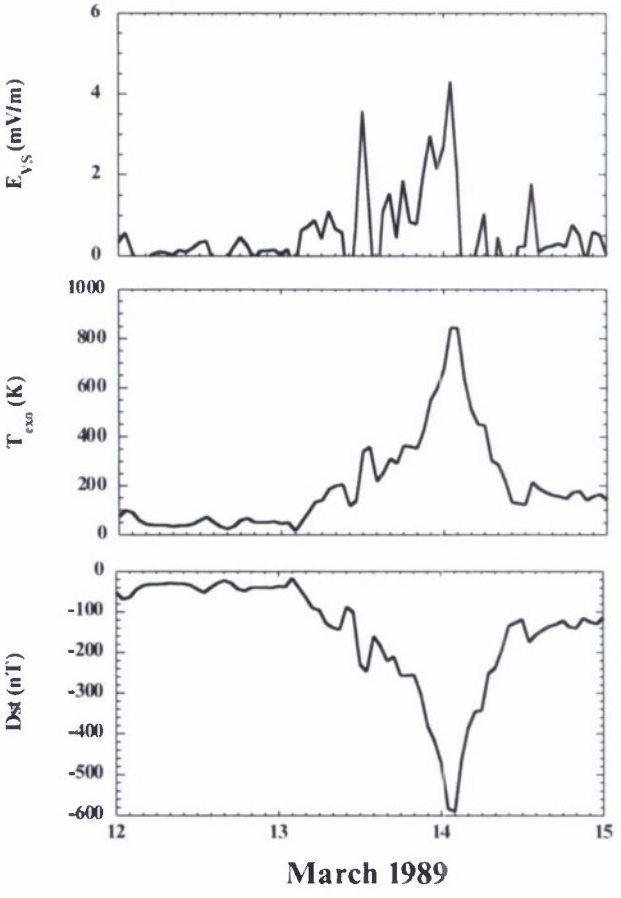

Figure 10. Model estimates of (top) ε_{VS} and (middle) $T_{\infty\ SW}$ driven by (bottom) Dst during the magnetic storm of March 1989.

[42] The three major new conclusions of this paper are.

[43] 1. Storm time energy increments to the global thermosphere are well represented as those of a driven-dissipative thermodynamic system.

[44] 2. Rates of electromagnetic energy inputs to the thermosphere consistent with $\overline{\rho}$ variations measured by GRACE match the independent predictions of the W5 model.

[45] 3. Since $T_{\infty\ SW}$ and Dst respond to the same ε_{VS} driver, quantitative estimates of changes in the storm time thermosphere can be extracted even when interplanetary data are unavailable.

[46] We close with a *caveat emptor*. During the research period leading up to the writing of this paper our access to reduced CHAMP and GRACE measurements was limited. Since the CHAMP data segment had significant gaps during magnetic storms, our analysis concentrated on measurements from GRACE during the summer and late fall of 2004. Thus this report is more an extended case study than a statistical analysis. Our estimate of $\alpha_E \approx 5.5 \cdot 10^{15}$ [(J/hr)/(mV/m)] relied solely on GRACE measurements acquired during the July 2004 storm period. With no adjustments this value also replicated GRACE-based estimates of $E_{th\ SW}$ during the November storms. Because α_E ε_{VS} and the independently determined P_{W5} are in substantial agreement during the two storm periods we regard this estimate as well grounded.

[47] That said, we also regard the stated value of α_E as approximate rather than definitive. The main reason for this assessment derives from the recent analysis of *Bowman et al.* [2008] who demonstrated that the independent calibrations of accelerometers on CHAMP and GRACE are irreconcilable. The calibration differences are not large. However, it will take time to reach consensus on the best *in situ* calibrations of the CHAMP and GRACE accelerometers.

Appendix A: Model of the Thermosphere of *Jacchia* [1977]

[48] J77 is a static model of thermospheric densities based on analytically defined temperature profiles. It approximates the upper atmosphere as being composed of N_2, O_2, O, He, and H with all species sharing the same temperature profiles. These gases are considered well mixed below 100 km and in diffusive equilibrium above it. The mesopause is set at the height z_o = 90 km where J77 imposes the boundary conditions: $\rho_{90} = 3.43 \times 10^{-9}$ g/cm^3, T_{90} = 188 K, and $dT_{90}/dz = 0$. At z_x = 125 km all temperature profiles have inflection points ($d^2T_x/dz^2 = 0$), where dT_x/dz is continuous. Above 125 km T increases and asymptotically approaches an exospheric temperature T_∞. Both the temperature T_x and dT_x/dz at the inflection point are functions of T_∞.

[49] In the J77 model the relationship between T_x and T_∞ is given by

$$T_x = 188 + 110.5 Sinh^{-1}[.0045(T_\infty - 188)] \quad \text{(A1)}$$

For $90 \le z \le 125$ km

$$T = T_x + A\tan^{-1}\left\{\frac{G_x}{A}(z - z_x)\left[1 + 1.7\left(\frac{(z - z_x)}{(z - z_0)}\right)^2\right]\right\} \quad \text{(A2)}$$

For $z \ge 125$ km

$$T = T_x + A\tan^{-1}\left\{\frac{G_x}{A}(z - z_x)\left[1 + 5.5 \cdot 10^{-5}(z - z_x)^2\right]\right\} \quad \text{(A3)}$$

where $G_x = 1.9(\frac{T_x - 188}{z_x - z_0})$ and $A = (2/\pi)(T_\infty - T_x)$.

[50] Above 100 km, densities of individual species n(i) are described by the diffusion equation

$$\frac{dn(i)}{n(i)} = -\frac{M_i g}{R^* T}dz - \frac{dT}{T}(1 + \alpha_i) \quad \text{(A4)}$$

where M_i is the molecular weight of the ith species, g is the local acceleration due to gravity, R* is the universal gas constant 8.31432 joules/(mole °K), and the thermal diffusion coefficient $\alpha_i = -0.38$ for helium and $\alpha_i = 0$ for other constituents.

Appendix B: Volland-Stern Electric Fields

[51] As formulated by *Ejiri* [1978] the Volland-Stern (V-S) model offers a simple, albeit limited, method for estimating the trajectories of ring current ions in the inner magnetosphere. One difficulty in applying the model concerned the connection between the interplanetary electric field (IEF) and its magnetospheric manifestations. *Burke* [2007] reformulated V-S by combining it with the Siscoe-Hill (S-H) model of the polar cap potential (Φ_{PC}) to show that in the absence of shielding the electric field in the inner magnetosphere is given by $\varepsilon_{VS} \approx \Phi_{PC}/2R_E L_Y$, where the denominator represents the width of the magnetosphere along the dawn-dusk line. This appendix outlines our method for calculating values of ε_{VS} used in the main text.

[52] Empirical studies suggest that on the dayside the equatorial magnetopause is nearly self-similar in shape with $L_Y \approx 1.5\ L_X$ [*Roelof and Sibeck*, 1993]. Force balance at the subsolar magnetopause requires that

$$L_X \approx \sqrt[6]{\frac{B_0^2}{\mu_0 P_{SW}}} \approx \frac{9.6}{\sqrt[6]{P_{SW}(nPa)}} \text{ and}$$
$$L_Y \approx 14.4/\sqrt[6]{P_{SW}(nPa)} \quad \text{(B1)}$$

More precise estimates of magnetopause dimensions that include erosion effects can be introduced where more rigorous calculations are required [*Yang et al.*, 2003].

[53] Between 1980 and 2000 many investigators sought linear relationships between Φ_{PC} and interplanetary parameters. *Burke et al.* [1999] surveyed published analyses of Φ_{PC} dependence on solar wind parameters and showed that in the linear regime, consistently high correlation coefficients were obtained with the relationship

$$\Phi_E(kV) = \Phi_0 + L_G V_{SW} B_T Sin^2\frac{\theta}{2} \quad \text{(B2)}$$

The subscript E refers to IEF contributions; Φ_0 is a residual potential with typical values between 20 and 30 kV, $B_T = \sqrt{(B_Y^2 + B_Z^2)}$, and $\theta = Cos^{-1}(B_Z/B_T)$ is the IMF clock angle in the Y-Z plane. The term $V_{SW}\ B_T\ Sin^2\ \theta/2$ roughly corresponds to ε_1 in equation (10) [*Burton et al.*, 1975]. If we express $V_{SW}\ B_T$ in kV/R_E (where 1 mV/m $\approx$ 6.4 kV/R_E)

then the regression slope L_G represents a 3 to 4 R_E wide "gate" in the solar wind through whieh geoeffeetive streamlines (equipotentials) must pass to reaeh the dayside magnetopause.

[54] *Siscoe et al.* [2002] suggested that during large magnetie storms Region 1 eurrents generate perturbation magnetie fields that alter the shape of the dayside magnetopause, thereby limiting aeeess of solar wind streamlines and foreing the merging rate to saturate. Following the suggestion of *Hill* [1984], *Siscoe et al.* [2002] postulated that a saturation potential Φ_S eontributes to Φ_{PC}

$$\Phi_{PC} = \frac{\Phi_E \Phi_S}{\Phi_E + \Phi_S} = \left(1 + \frac{\Phi_E}{\Phi_S}\right)^{-1} g\left(\Phi_0 + L_G V_{SW} B_T \mathrm{Sin}^2 \frac{\theta}{2}\right)$$
$$= \xi(\Phi_E, \Phi_S) g\left(\Phi_0 + L_G V_{SW} B_T \mathrm{Sin}^2 \frac{\theta}{2}\right) \quad \text{(B3)}$$

Note that when $\Phi_E \ll \Phi_S$, $\Phi_{PC} \rightarrow \Phi_E$, and the standard linear relation equation (B2) is retrieved. Sinee the ratio $\Phi_E/\Phi_S > 0$, $\xi(\Phi_E, \Phi_S) < 1$. We define the width of the storm time geoeffeetive gate as $L_{GS} = \xi(\Phi_E, \Phi_S)\, L_G$. Sinee $\varepsilon_{VS} = \Phi_{PC}/2L_Y R_E$, the ratio $\varepsilon_I/\varepsilon_{VS} \approx 2L_Y/L_{GS}$. Beeause L_{GS} is a funetion of ε_I the ratio of interplanetary to magnetospherie eleetrie fields is inherently nonlinear. No single ratio deseribes all situations.

[55] *Siscoe et al.* [2002] derived an expression for Φ_S in kV.

$$\Phi_S(kV) = \frac{1600 \sqrt[3]{P_{SW}(nPa)}}{\Sigma_P(mho)} \quad \text{(B4)}$$

where P_{SW} is the dynamie pressure of the solar wind and Σ_P is the effeetive Pedersen eonductance of the polar ionosphere. *Ober et al.* [2003] used data from the SWEPAM and MFI on ACE to eompare Φ_{PC} predietions of the S-H and other models with DMSP measurements during the magnetie storm of Mareh 2001. Under prestorm eonditions all of the models predieted Φ_{PC} values measured by DMSP. During the main phase S-H predietions of Φ_{PC} provided an exeellent, upper bound envelope for DMSP observations. Linear models predieted mueh larger than observed Φ_{PC}. *Burke et al.* [2007b] found that setting Σ_P = 10 mho provided exeellent agreement between ealeulated and observed Φ_{PC} during a large number of magnetie storms.

[56] In eomputations of ε_{VS} we used hourly averaged values of the solar wind density and veloeity from SWEPAM and IMF eomponents in solar-magnetospherie eoordinates from the MFI on ACE. In applieations to Siseoe-Hill we set Φ_0 = 25 kV, L_G = 3.5 and Σ_P = 10 mho.

[57] **Acknowledgments.** Support for the presented work was provided by the Air Force Office of Scientific Research, Task 2311SDA3, and AF contract FA8718-08-C-0012 with Boston College. The authors thank Brian D. Tapley of the University of Texas for use of the reduced GRACE measurements that form the empirical basis of this report.

[58] Amitava Bhattacharjee thanks the reviewers for their assistance in evaluating this paper.

References

Bowman, B. R., W. K. Tobiska, and F. A. Marcos (2006), A new empirical thermospheric density model JB2006 using new solar indices, *AIAA Astrodynamics Conference*, Keystone, Colo., *AIAA 2006-6166*.

Bowman, B. R., W. K. Tobiska, F. A. Marcos, C. Y. Huang, C. S. Lin, and W. J. Burke (2008), A new empirical thermospheric density model JB2008 using new solar and geomagnetic indices, *Astrodynamic Specialist Conference*, Honolulu, Hawaii, *AIAA 2008-6438*.

Bruinsma, S., and R. Biancale (2003), Total densities derived from accelerometer data, *J. Spacecraft Rockets*, *40*, 230–236.

Bruinsma, S., D. Tamagnan, and R. Biancale (2004), Atmospheric densities derived from CHAMP/STAR accelerometer observations, *Planet. Space Sci.*, *52*, 297–312.

Burke, W. J. (2007), Penetration electric fields: A Volland-Stem approach, *J. Atmos. Sol. Terr. Phys.*, *69*, 1114–1126.

Burke, W. J. (2008), Stormtime energy budgets of the global thermosphere, in *Mid-Latitude Ionospheric Dynamics and Disturbances*, *Geophys. Monogr. Ser.*, vol. 181, edited by P. M. Kintner et al., pp. 235–246, AGU, Washington, D. C.

Burke, W. J., D. R. Weimer, and N. C. Maynard (1999), Geoeffective interplanetary scale sizes derived from regression analysis of polar cap potentials, *J. Geophys. Res.*, *104*, 9989.

Burke, W. J., C. Y. Huang, F. A. Marcos, and J. O. Wise (2007a), Interplanetary control of thermospheric densities during large magnetic storms, *J. Atmos. Sol. Terr. Phys.*, *69*, 279–287.

Burke, W. J., L. C. Gentile, and C. Y. Huang (2007b), Penetration electric fields driving main-phase Dst, *J. Geophys. Res.*, *112*, A07208, doi:10.1029/2006JA012137.

Burton, R. K., R. L. McPherron, and C. T. Russell (1975), An Empirical relationship between interplanetary conditions and Dst, *J. Geophys. Res.*, *80*, 4204.

Carovillano, R. L., and G. L. Siscoe (1973), Energy and momentum theorems in magnetospheric processes, *Rev. Geophys.*, *11*, 289.

Casali, S. J., and W. N. Barker (2002), Dynamic calibration atmosphere (DCA) tool for the high accuracy satellite drag model (HASDM), *AAS/AIAA Astrodynamics Speciolist Conference*, Monterey, Calif., *AIAA 2002-4888*.

Ejiri, M. (1978), Trajectory traces of charged particles in the magnetosphere, *J. Geophys. Res.*, *83*, 4798.

Hill, T. W. (1984), Magnetic coupling between solar wind and magnetosphere: Regulated by ionospheric conductance, *Eos Trans. AGU*, *65*, 1047.

Huang, C. Y., and W. J. Burke (2004), Transient sheets of field-aligned current observed by DMSP during the main phase of a magnetic storm, *J. Geophys. Res.*, *109*, A06303, doi:10.1029/2003JA010067.

Jacchia, L. G. (1977), Thermospheric temperature, density and composition: A new model, *SAO Spec. Rep. 375*, 15 March.

Knipp, D. J., W. K. Tobiska, and B. A. Emery (2005), Direct and indirect thermospheric heating sources for solar cycles 21–23, *Sol. Phys.*, *224*, 495–505.

Marcos, F. A., M. J. Kendra, J. M. Griffin, J. N. Bass, D. R. Larson, and J. J. Liu (1998), Precision low Earth orbit determination using atmospheric density calibration, *J. Astronaut. Sci.*, *6*, 395–409.

McComas, D. J., S. J. Bame, P. Barber, W. C. Fieldman, J. L. Phillips, and P. Riley (1998), Solar wind electron, proton, and alpha monitor (SWEPAM) on the Advanced Composition Explorer, *Space Sci. Rev.*, *86*, 563–612.

Mlynczak, M. G., et al. (2005), Energy transport in the thermosphere during the solar storms of April 2002, *J. Geophys. Res.*, *110*, A12S25, doi:10.1029/2005JA011141.

Ober, D. M., N. C. Maynard, and W. J. Burke (2003), Testing the Hill model of transpolar potential saturation, *J. Geophys. Res.*, *108*(A12), 1467, doi:10.1029/2003JA010154.

Roelof, E. C., and D. G. Sibeck (1993), Magnetopause shape as a bivariate function of interplanetary magnetic field Bz and solar wind dynamic pressure, *J. Geophys. Res.*, *98*, 21,241.

Siscoe, G. L., G. M. Erickson, B. U. Ö. Sonnerup, N. C. Maynard, J. A. Schoendorf, K. D. Siebert, D. R. Weimer, W. W. White, and G. R. Wilson (2002), Hill model of transpolar potential saturation: Comparison with MHD simulation, *J. Geophys. Res.*, *107*(A6), 1075, doi:10.1029/2001JA000109.

Smith, C. W., M. H. Acuna, L. F. Burlaga, J. L. L'Heureux, N. F. Ness, and J. Scheifele (1998), The ACE magnetic field experiment, *Space Sci. Rev.*, *86*, 613–630.

Stern, D. P. (2005), A historical introduction to the ring current, in *The Inner Magnetosphere: Physics and Modeling*, *Geophys. Monogr. Ser.*, vol. 155, edited by T. I. Pulkkinen, N. A. Tsyganenko, and R. H. W. Friedel, p. 1, AGU, Washington, D. C.

Tapley, B. D., S. Bettadpur, M. Watkins, and C. Reigber (2004), The gravity recovery and climate experiment: Mission overview and early results, *Geophys. Res. Lett.*, *31*, L09607, doi:10.1029/2004GL019920.

Temerin, M., and X. Li (2002), A new model for the prediction of Dst on the basis of the solar wind, *J. Geophys. Res.*, *107*(A12), 1472, doi:10.1029/2001JA007530.

Temerin, M., and X. Li (2006), Dst model for 1995–2002, *J. Geophys. Res.*, *111*, A04221, doi:10.1029/2005JA011257.

Weimer, D. R. (2005), Improved ionospheric electrodynamic models and application to calculating Joule heating rates, *J. Geophys. Res.*, *110*, A05306, doi:10.1029/2005JA010884.

Weimer, D. R., D. M. Ober, N. C. Maynard, W. J. Burke, M. R. Collier, D. J. McComas, T. Nagai, and C. W. Smith (2002), Variable time delays in the propagation of the interplanetary magnetic field, *J. Geophys. Res.*, *107*(A8), 1211, doi:10.1029/2001JA009102.

Wilson, G. R., D. R. Weimer, J. O. Wise, and F. A. Marcos (2006), Response of the thermosphere to Joule heating, *J. Geophys. Res.*, *111*, A10314, doi:10.1029/2006JA011274.

Wright, D. (2007), Space debris, *Phys. Today*, *60*(10), 35–40.

Wygant, J., D. Rowland, H. J. Singer, M. Temerin, F. Mozer, and M. K. Hudson (1998), Experimental evidence on the role of the large spatial scale electric field in creating the ring current, *J. Geophys. Res.*, *103*, 29,527.

Yang, Y.-H., J. K. Shoa, A. V. Dmitriev, C.-H. Lin, and D. M. Ober (2003), Saturation of IMF Bz influence on the position of dayside magnetopause, *J. Geophys. Res.*, *108*(A3), 1104, doi:10.1029/2002JA009621.

Young, H. D. (1992), *Physics*, 8th ed., pp. 874–878, Addison Wesley, Reading, Mass.

W. J. Burke, C. Y. Huang, C. S. Lin, F. A. Marcos, and J. O. Wise, Air Force Research Laboratory, Space Vehicles Directorate, 29 Randolph Road, Hanscom, MA 01731-3010, USA.

L. C. Gentile and M. P. Hagan, Institute for Scientific Research, Boston College, 402 St. Clement's Hall, 140 Commonwealth Avenue, Chestnut Hill, MA 02467-3862, USA.

D. R. Weimer, Virginia Tech National Institute of Aerospace, 100 Exploration Way, Hampton, VA 23666, USA.